J Mater Sci (2009) 44:821–827
DOI 10.1007/s10853-008-3151-7

Photocatalytic degradation of methylene blue by Au-deposited TiO_2 film under UV irradiation

Chihiro Yogi · Kazuo Kojima · Tomoo Takai · Noriyuki Wada

Received: 17 July 2008 / Accepted: 2 December 2008 / Published online: 27 December 2008

Abstract A TiO_2 photocatalytic film was prepared by the sol–gel and dip-coating methods. Au-loaded TiO_2 photocatalytic films were produced by the photodeposition method. The photocatalytic activity of the films under UV irradiation was evaluated by measuring the degradation of absorbance for a methylene blue (MB) aqueous solution. Au particles deposited on the TiO_2 film improved the photocatalytic activity under the O_2 bubbling condition. On the other hand, under N_2 or Ar bubbling, the doubly reduced form of MB, *leuco*-methylene blue (LMB), was formed at the beginning of UV irradiation, and then both MB and LMB were decomposed gradually by the photocatalytic reaction. In this process, Au particles on the TiO_2 film behave as electron traps.

Introduction

Metal particles such as Ag, Pt, and Au have been reported to enhance the photocatalytic performance of TiO_2, because the photogenerated electrons are trapped by these particles leading to high efficiency of charge separation [1–6]. The mechanism of the improvement of the photogenerated electron-hole separation is the shift in the Fermi level followed by charge distribution in semiconductor–metal composite under UV irradiation. Wood et al. [7] suggested that the process of Fermi level equilibration was monitored using changes to both the surface plasmon band of the metal island and the sharp exciton band of the ZnO nanocrystals. Kamat and co-workers showed that the green and blue colors of UV-irradiated ZnO [8] and TiO_2 [9] semiconductors were removed by the deposition of Au nanoparticles, indicating that the stored electrons in semiconductors were transferred to Au nanoparticles, which caused the negative shift in the Fermi level.

In this study, we measured the photocatalytic degradation of a methylene blue (MB) aqueous solution by a TiO_2 film prepared by the sol–gel and dip-coating methods and Au nanoparticles-loaded TiO_2 films prepared by the photodeposition method, under aerobic (O_2 bubbling) and anaerobic (N_2 and Ar bubbling) conditions, and discussed the effect of Au particles.

Experimental

Preparation of photocatalytic films of TiO_2 and Au-deposited TiO_2

A TiO_2 photocatalytic film was prepared by a sol–gel method. The mole ratio of the reagents used for preparing a sol solution was $Ti(O–i–C_3H_7)_4$:H_2O (distilled water):C_2H_5OH:$NH(C_2H_4OH)_2$ = 1:4:40:1. Firstly, $NH(C_2H_4OH)_2$ and a half amount of C_2H_5OH were mixed for 30 min, followed by adding $Ti(O–i–C_3H_7)_4$ with stirring for 30 min at room temperature (solution A). Another solution B, prepared by mixing the remaining C_2H_5OH with H_2O, was added to

C. Yogi · K. Kojima (✉) · T. Takai
Department of Applied Chemistry, Faculty of Science and Engineering, Ritsumeikan University, 1-1-1 Noji-higashi, Kusatsu, Shiga 525-8577, Japan
e-mail: kojimaka@sk.ritsumei.ac.jp

N. Wada
Department of Materials Science and Engineering, Suzuka National College of Technology, Shiroko, Suzuka, Mie 510-0294, Japan

the solution A with stirring for 30 min at 0 °C, followed by additional stirring for 60 min. A quartz glass substrate ($9 \times 70 \times 1$ mm^3) was dipped into the resulting sol solution, and then drawn up at the rate of 0.3 mm/s, followed by drying at 100 °C for 10 min. This process was repeated and the resulting gel film was heated from 100 to 500 °C within 30 min and kept at 500 °C for 60 min. These coating and heat-treatment processes were repeated four times to obtain totally 8-fold coating film (9×60 mm^2).

Au particles were loaded on the TiO_2 film surface by photodeposition. A 6-fold coating film was dip-coated one time and dried for 30 min at RT, followed by dip-coating again for one last time (totally 8-fold coating). Immediately after the last dip-coating, the film was immersed into 13 mL of a 0.25-mM $HAuCl_4$ aqueous solution in a quartz cell ($10 \times 25 \times 60$ mm^3). This $HAuCl_4$ solution was irradiated by a Spectronics ENF-260C/J UV lamp (365 nm; 100 μW/cm^2) for 15, 45, or 60 min to deposit Au particles on the surface of the TiO_2 film in the solution. The resulting Au-deposited film was heated from 100 to 500 °C within 30 min and kept at 500 °C for 60 min. The films obtained by irradiation of 15, 45, and 60 min will be hereafter abbreviated as 15Au–TiO_2, 45Au–TiO_2, and 60Au–TiO_2, respectively.

Characterization and photocatalytic activity measurement

UV–Vis absorption spectra of the films were recorded on a Shimadzu UV-365 UV–Vis spectrophotometer. X-ray diffraction (XRD, Rigaku RINT/DMAX-2000 X-ray diffractometer with Cu-Kα radiation) measurements were carried out to characterize the crystalline phase. The accelerating voltage and the applied current were 40 kV and 20 mA, respectively. Surface and cross-sectional morphologies of the films were observed by using field-emission scanning electron microscope (FE-SEM, Hitachi S-4800). Energy dispersive X-ray spectroscopy (EDX, HORIBA EMAX-7000) was performed to determine the existence of Au on the TiO_2 films. Transmission electron microscopy (TEM) and selected-area electron diffraction (SED) images, which were all obtained by means of a JEOL JEM-2100 at the acceleration voltage of 200 kV, were used to observe or determine the morphology, crystallite size, and to identify nanocrystal particles in the films. An MB aqueous solution of 8.12 μM was photocatalyzed in a quartz cell ($10 \times 10 \times 45$ mm^3) at 25 °C. The TiO_2 or Au-deposited TiO_2 film immersed in the solution was irradiated by the 365-nm UV lamp (130 μW/cm^2). A Shimadzu UV-1700 UV–Vis spectrophotometer was used to measure absorption spectra of the MB aqueous solution as a function of the 365-nm UV irradiation time. The MB aqueous solution was bubbled with O_2, N_2, or Ar for 20 min prior to UV irradiation and the bubbling was continued during irradiation.

Results

Characterization

The TiO_2 film was colorless, while the color of the Au-deposited TiO_2 film was changed from blue to dark blue by increasing the time of UV irradiation for the $HAuCl_4$ solution. These colors are due to the surface plasmon absorption (about 640 nm, Fig. 1) of Au metal particles that were produced from the reduction of Au^{3+} ions in the $HAuCl_4$ solution by photocatalyzation of the TiO_2 film under 365-nm UV irradiation. Figure 1 also shows the absorption edge of ca. 380 nm, meaning the 3.2 eV band gap of anatase TiO_2. XRD patterns (Fig. 2) show that the films are composed of anatase TiO_2 and that cubic Au exists in the Au–TiO_2 films. From the Scherrer equation, the crystallite sizes of anatase TiO_2 were estimated to be ca. 19 nm, hardly dependent on the type of the films. The crystallite sizes of Au on the TiO_2 films are 25 nm (15Au–TiO_2), 24 nm (45Au–TiO_2), and 23 nm (60Au–TiO_2), respectively. Figure 3 gives TEM and SED images of the 45Au–TiO_2 film. The corresponding SED patterns reveal that the film is composed of anatase TiO_2 nanocrystals with Au particle over it. The crystallite size of anatase TiO_2, ranged from 5 to 15 nm, was in agreement with the XRD result. This film also possesses Au particles; the spots of Au also appear in SED image, the size of Au

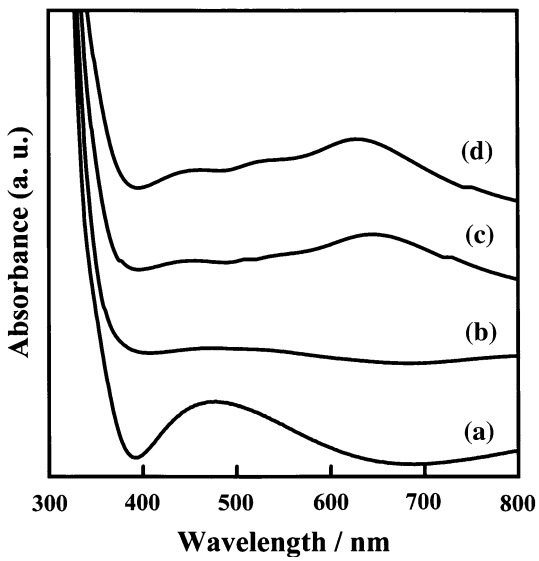

Fig. 1 UV–Vis absorption spectra of films: (a) TiO_2, (b) 15Au–TiO_2, (c) 45Au–TiO_2, and (d) 60Au–TiO_2

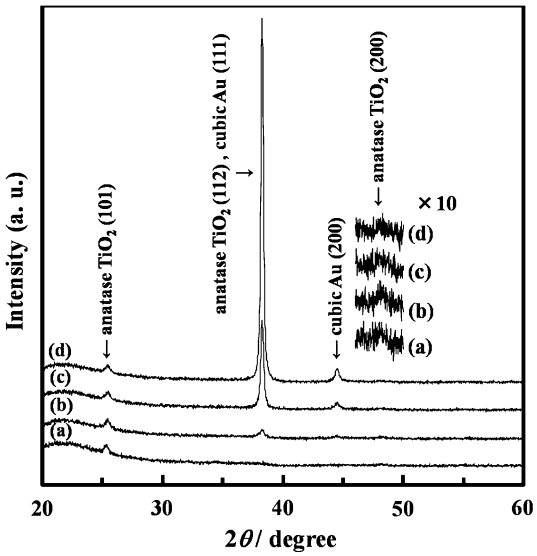

Fig. 2 XRD patterns of films: (a) TiO_2, (b) 15Au–TiO_2, (c) 45Au–TiO_2, and (d) 60Au–TiO_2

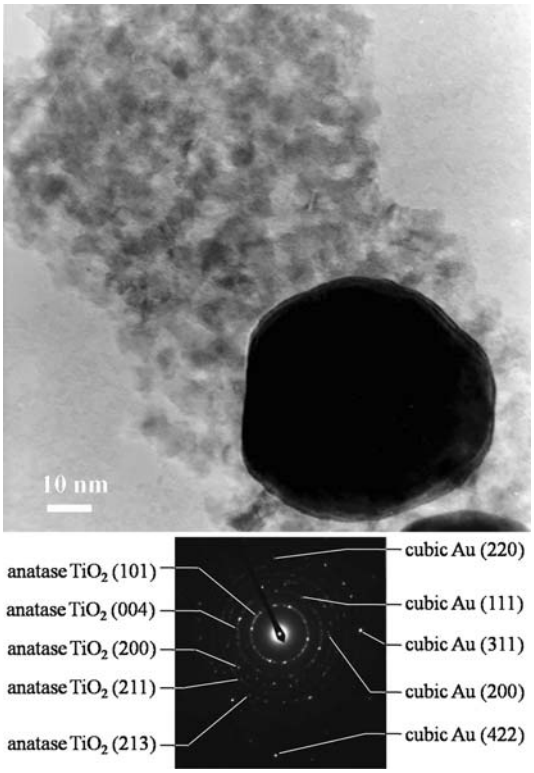

Fig. 3 TEM and SED images of the 45Au–TiO_2 film

being in the range of its particle size distribution as will be shown below. Figures 4 and 5 show FE-SEM images of the film surfaces and EDX liner analysis of the 45Au–TiO_2 film surface, respectively. From EDX analysis, the bright spots in the FE-SEM images correspond to Au particles. The size distributions of the Au particle are also shown in Fig. 4, the wide distribution of the Au particles being observed on the TiO_2 film surface. The results of FE-SEM and XRD indicate that the Au particles obtained were highly aggregated. From the FE-SEM images of the cross sections, the film thickness is evaluated as follows: 157 nm (TiO_2), 149 nm (15Au–TiO_2), 188 nm (45Au–TiO_2), and 170 nm (60Au–TiO_2). The cross-sectional image of the 45Au–TiO_2 film is shown in Fig. 6 as an example.

Photocatalytic activity

Figure 7 shows absorption spectral changes of the MB aqueous solutions when the solutions were photocatalytically degraded by the TiO_2 and Au-deposited TiO_2 films under bubbling O_2, N_2, or Ar. Figure 8 gives the UV irradiation time dependence of the relative absorbance (A_t/A_0) at the absorption maximum wavelength of 665 nm for MB under O_2 and Ar bubbling, whereas the value of A_t/A_0 was obtained from Fig. 7. Under O_2 bubbling, it is found that compared with the TiO_2 film, the Au-deposited films improve the photocatalytic activity with less dependence on the amount of the deposition of Au. The maximum peak positions around 600–650 nm in Fig. 7A show blue shifts with increasing irradiation time. On the other hand, under Ar bubbling, the decrease in absorbance is steep at the beginning of 20 min of irradiation, and then becomes gentle, regardless of the films. The decrease tends to be low for the TiO_2 film, and high for the 45Au–TiO_2 film throughout the irradiation of 120 min.

Discussion

When TiO_2 absorbs light of energy greater than its band-gap energy (3.2 eV) in an aerobic (O_2 bubbling) aqueous solution, the following reactions associated with holes and electrons are reported to occur [10–15]:

$$TiO_2 + h\nu(\text{UV light}) \rightarrow TiO_2^*\left(e_{CB}^- + h_{VB}^+\right), \quad (1)$$

$$H_2O + h_{VB}^+ \rightarrow OH^\bullet + H^+, \quad (2)$$

$$OH_{ad}^- + h_{VB}^+ \rightarrow OH_{ad}^\bullet, \quad (3)$$

$$e_{CB}^- + O_2 \rightarrow O_2^{\bullet -}, \quad (4)$$

$$MB + \left(OH_{ad}^\bullet, OH^\bullet, O_2^{\bullet -}, h_{VB}^+\right) \rightarrow \text{degraded products}, \quad (5)$$

where TiO_2^* is TiO_2 in the excited state, OH_{ad}^- an adsorbed OH^-, e_{CB}^- a photoexcited electron in the conduction band, and h_{VB}^+ a photogenerated hole in the valence band. $OH^\bullet$ and $O_2^{\bullet -}$ produced in reactions (2) and (4) are highly active oxidizing species, so that they are considered to contribute greatly to photocatalysis of decomposing various types of

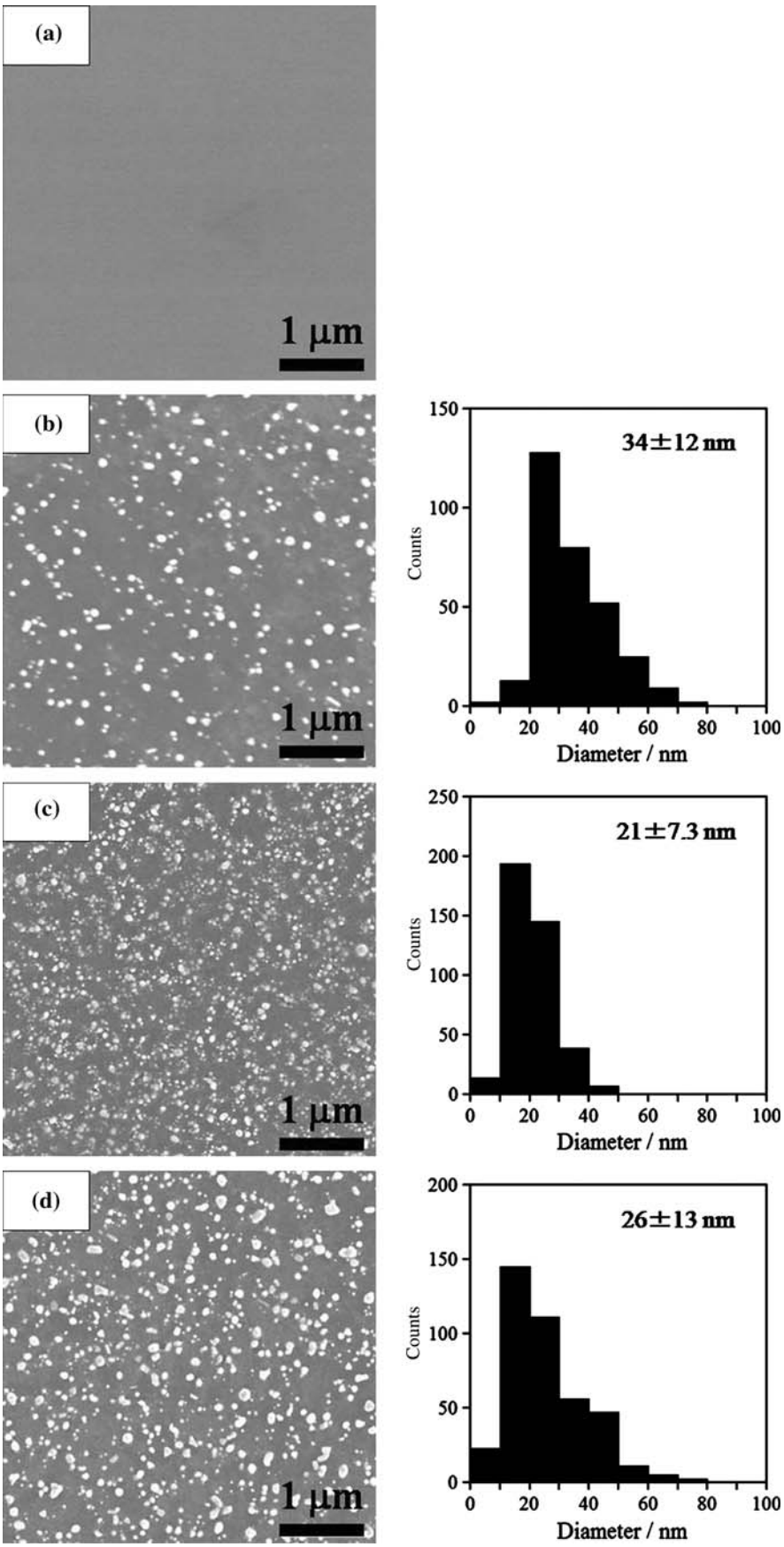

Fig. 4 FE-SEM images of film surfaces and size distributions of Au particles: (**a**) TiO_2, (**b**) 15Au–TiO_2, (**c**) 45Au–TiO_2, and (**d**) 60Au–TiO_2

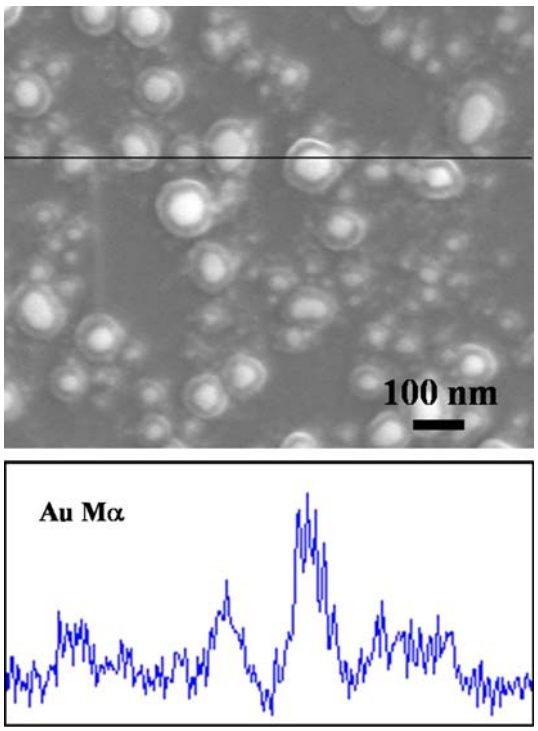

Fig. 5 EDX liner analysis of the 45Au–TiO_2 films surface

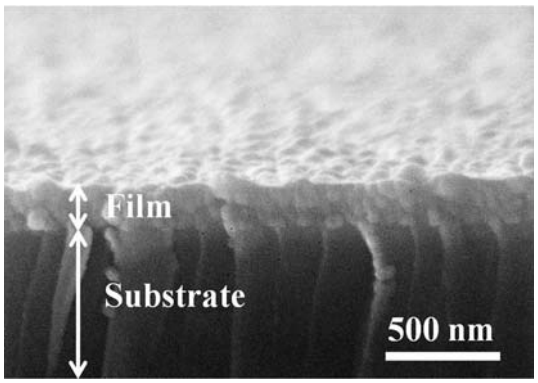

Fig. 6 Cross-sectional images of the 45Au–TiO_2 film

organic compounds. It is thought that in the Au-deposited TiO_2 film, e^-_{CB} accumulates in the Au particles to yield Au(e^-) (reaction (6)), which leads to depress the electron–hole recombination. Then Au(e^-) is trapped by oxygen to produce the active $O_2^{\bullet -}$ by reaction (7). This is the reason why the Au-deposited films give high photocatalytic activity in this study, as shown in Fig. 8a. The maximum peak positions around 600–650 nm in Fig. 5a show blue shifts with increasing UV irradiation time, which is due to the demethylation reaction of MB. Therefore, the photodegradation and demethylation reactions occur simultaneously [12, 16].

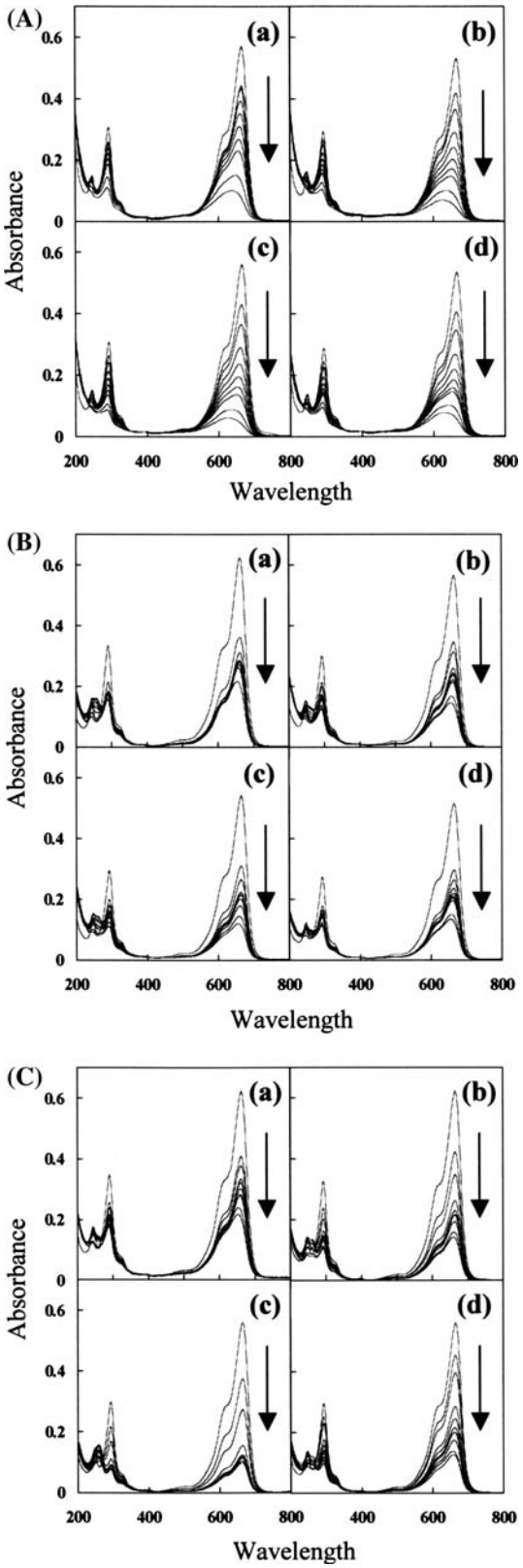

Fig. 7 Absorption spectral changes of MB aqueous solution degraded by photocatalytic films under bubbling of O_2 (**A**), N_2 (**B**), and Ar (**C**) for 120 min: (a) TiO_2, (b) 15Au–TiO_2, (c) 45Au–TiO_2, and (d) 60Au–TiO_2

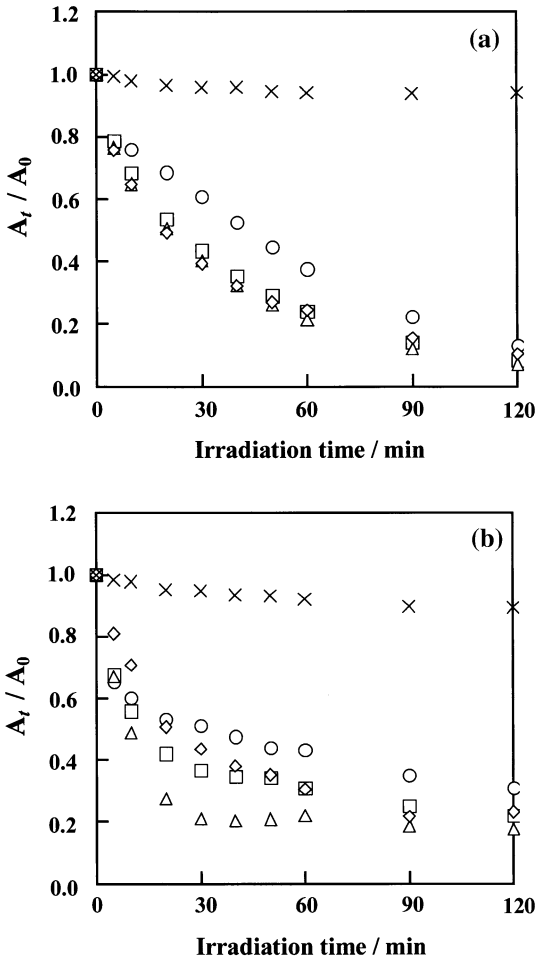

Fig. 8 Relative absorbance at 665 nm in absorption spectra of MB aqueous solution under bubbling of O_2 (**a**) and Ar (**b**): ◯ TiO_2, □ 15Au-TiO_2, △ 45Au-TiO_2, ◇ 60Au-TiO_2, and × none

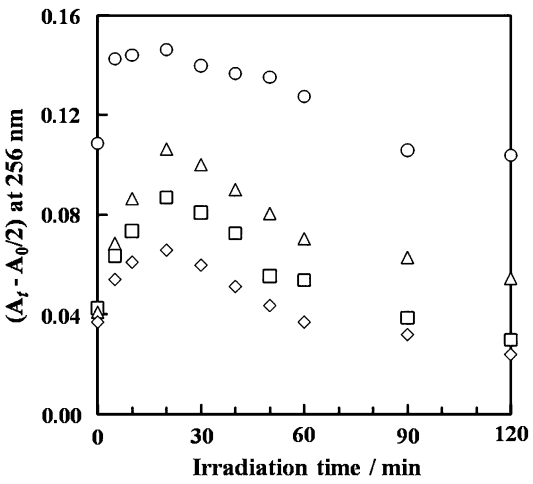

Fig. 9 Peak absorbance at 256 nm in absorption spectra of MB aqueous solution under Ar bubbling: ◯ TiO_2, □ 15Au-TiO_2, △ 45Au-TiO_2, and ◇ 60Au-TiO_2

$$Au + e^-_{CB} \rightarrow Au(e^-), \quad (6)$$

$$Au(e^-) + O_2 \rightarrow O_2^{\bullet -}. \quad (7)$$

On the other hand, in an anaerobic condition (N_2 and Ar bubbling), the following reactions associated with electrons are considered to occur [17]:

$$MB + e^-_{CB} \rightarrow MB^{\bullet -} \text{or } MB + Au(e^-) \rightarrow MB^{\bullet -}, \quad (8)$$

$$2MB^{\bullet -} \rightarrow MB + LMB, \quad (9)$$

$$MB^{\bullet -} + 2e^-_{CB} + H^+ \rightarrow LMB. \quad (10)$$

MB serves as an acceptor for e^-_{CB} to produce semi-reduced MB, $MB^{\bullet -}$, in reaction (8). This $MB^{\bullet -}$ disproportionates to form MB and the doubly reduced form of MB, *leuco*-methylene blue (LMB), in reaction (9), or it reacts with e^-_{CB} and H^+ to yield LMB in reaction (10). The above reaction (2) associated with holes occurs in this aqueous solution too, therefore H^+ in reaction (10) may be supplied by reaction (2). The formation of LMB is confirmed by the appearance of an absorption peak at 256 nm in Fig. 7B, C. To find the concentration change of LMB, we obtained the absorbance difference at 256 nm, $A_t - (A_0/2)$, in Fig. 7C and plotted it as a function of the UV irradiation time in Fig. 9, where half the absorbance of the MB solution at 256 nm at the irradiation time of zero; $A_0/2$, was selected as a tentative base point because the base lines of the spectra were considerably shifted with the UV irradiation time as seen in Fig. 7C. Figure 9 reveals that the concentration of LMB shows a maximum at about 20 min, and then decreases gradually in the case of the Au–TiO_2 films. A similar tendency was observed under N_2 bubbling in Fig. 7B. Comparing Fig. 8b with Fig. 7, it is clear that the step-like decrease in absorbance at the beginning of 20 min of irradiation shown in Fig. 8b is mainly due to the formation of LMB by reactions (9) and (10). Even under N_2 and Ar bubbling, the photodegradation and demethylation reactions may occur simultaneously due to the active species of $OH^{\bullet}_{ad}$ and $OH^{\bullet}$ produced from reactions (2) and (3). However, the demethylation reaction is considered to hardly occur during the formation of LMB [16] because the maximum peak positions around 600–650 nm in Fig. 7B and C are found to be scarcely blue-shifted. The gradual decrease after the irradiation time of 20 min is due to the photodegradation of both MB and LMB. Compared to the Au–TiO_2 film, the absorbance at 256 nm does not increase for the TiO_2 film; the increase in absorbance in the initial 5 min is due to an increase in the base line. In other words, the Au–TiO_2 film generated much more LMB than the TiO_2 film under N_2 or Ar bubbling condition, which is reinforced by the reactions (8–10). Therefore, it is suggested that Au particles behave as electron traps. Under the O_2 bubbling condition, the

reactions (8–10) as well as reaction (4) probably occur concomitantly; however, the former reactions may be inferior to the latter one, resulting in no observation of LMB in Fig. 7A.

Conclusion

Au-loaded TiO_2 photocatalytic films were prepared by the photodeposition method. The photocatalytic activity of the films under UV irradiation was evaluated by using the MB aqueous solution. Au particles promote the charge separation of electrons and holes generated in TiO_2, and improve the photocatalytic activity under the O_2 bubbling condition. Under N_2 or Ar bubbling, the absorbance of MB is reduced steeply due to the formation of LMB at the beginning of UV irradiation, and Au particles on the TiO_2 film behave as electron traps, which facilitates the generation of LMB.

Acknowledgements This study is supported by the Nishio Scholarship. We also thank Dr. Hashishin, Department of Applied Chemistry, College of Life Sciences, Ritsumeikan University, for discussion in respect of TEM analysis.

References

1. Arabatzis IM, Stergiopouls T, Andreeva D, Kitova S, Neophytides SG, Falaras P (2003) J Catal 220:127
2. Orlov A, Jefferson DA, Macleod N, Lambert RM (2004) Catal Lett 92:41
3. Li J, Zeng HC (2006) Chem Mater 18:4270
4. Sonawane RS, Dongare MK, Mol J (2006) Catal A Chem 243:68
5. Yu J, Xiong J, Cheng B, Liu S (2005) Appl Catal B Environ 60:211
6. Iliev V, Tomova D, Todorovska R, Oliver D, Petrov L, Todorovsly D, Uzunova-Bujnova M (2006) Appl Catal A Gen 313:115–121
7. Wood A, Giersig M, Mulvaney P (2001) J Phys Chem B 105:8810
8. Subramanian V, Wolf EE, Kamat PV (2003) J Phys Chem B 107:7479
9. Hakob M, Levanon H, Kamat PV (2003) Nano Lett 3:353
10. Lee B, Liaw W, Lou J (1999) Environ Eng Sci 16:165
11. Lakshmi S, Renganathan R, Fujita S (1999) J Photochem Photobiol A Chem 127:123
12. Li X, Liu G, Zhao J (1999) New J Chem 23:1193
13. Tacconi NR, Carmona J, Rajeswar K (1997) J Electrochem Soc 144:2486
14. Tatsuma T, Tachibana S, Miwa T, Trky DA, Fujishima A (1999) J Phys Chem B 103:8033
15. Ma Y, Yao J (1999) Chemosphere 38:2407
16. Zhang T, Oyama T, Aoshima A, Hidaka H, Zhao J, Serpone N (2001) J Photochem Photobio A Chem 140:163
17. Mills A, Wang J (1999) J Photochem Photobiol A Chem 27:123